

THE UNORTHODOX ORBITS OF SUBSTRUCTURE HALOS

AARON D. LUDLOW^{1,6}, JULIO F. NAVARRO^{1,2}, VOLKER SPRINGEL³, ADRIAN JENKINS⁴,
CARLOS S. FRENK⁴, AMINA HELMI⁵

¹ Department of Physics and Astronomy, University of Victoria, 3800 Finnerty Rd., Victoria, BC, V8P 5C2, Canada

² Astronomy Department, University of Massachusetts, 710 N. Pleasant St., Amherst, MA 01003, USA

³ Max-Planck Institute for Astrophysics, Karl-Schwarzschild Str. 1, D-85748, Garching, Germany

⁴ Institute of Computational Cosmology, Department of Physics, University of Durham, Science Laboratories, South Road, Durham, DH1 3LE, UK and

⁵ Kapteyn Institute, P.O. Box 800, 9700 AV Groningen, The Netherlands

Draft version January 15, 2019

ABSTRACT

We use a suite of cosmological N-body simulations to study the properties of substructure halos (subhalos) in galaxy-sized cold dark matter halos. We extend prior work on the subject by considering the whole population of subhalos *physically associated* with the main system. These are defined as subhalos that have at some time been within the virial radius of the main progenitor and have survived as self-bound entities to $z = 0$. We find that this population extends beyond *three times* the virial radius, and contains objects on extreme orbits, with some approaching the nominal escape speed from the system. We trace the origin of these unorthodox orbits to multiple-body interactions acting during the tidal dissociation of bound groups of subhalos. Multiple-body interactions affect primarily low-mass subhalos, and push them onto higher energy orbits than their more massive counterparts. This results in a strong mass-dependent bias in the spatial distribution and kinematics of associated subhalos: the lower the subhalo mass at accretion time, the less centrally concentrated and kinematically hotter their descendant population. Our findings imply that subhalos identified within the virial radius represent a rather incomplete census of the substructure physically related to a halo: only about *one half* of all associated subhalos are found today within the virial radius of a halo, and many relatively isolated halos may have actually been ejected in the past from a more massive system. These results may explain the age dependence of the clustering of low-mass halos, and has implications for (i) the interpretation of the structural parameters, and assembly histories of halos neighboring massive systems; (ii) the existence of dynamical outliers, such as Leo I and And XII in the Local Group; and (iii) the presence of evidence for evolutionary effects, such as tidal truncation or ram-pressure stripping, well outside the traditional virial boundary of a system.

Subject headings: cosmology: dark matter – methods: N-body simulations – galaxies: kinematics and dynamics – galaxies: halos

1. INTRODUCTION

In the current paradigm of structure formation, the concordance Λ CDM scenario, the dark matter halos that host galaxy systems are assembled hierarchically, through the merger and accretion of smaller subunits. One relic of this process is the presence of *substructure*, which consists of the self-bound cores of accreted subsystems that have so far escaped full disruption in the tidal field of the main halo (Klypin et al 1999; Moore et al 1999).

Although substructure halos (referred to hereafter as “subhalos”, for short) typically make up only a small fraction (5 to 10%) of the total mass of the system, they chart the innermost regions of accreted subsystems, and are thus appealing tracers of the location and kinematics of the *galaxies* that the subhalos may have hosted. Substructure is thus a valuable tool for studying galaxies embedded in the potential of a much larger system, such as satellite galaxies orbiting a primary, or individual galaxies orbiting within a group or cluster of galaxies.

This realization has prompted a number of studies over the past few years, both analytical and numerical, aimed at characterizing the main properties of subhalos, such as

their mass function, spatial distribution, and kinematics (e.g. Ghigna et al 1998, 1999; Moore et al 1999; Taylor & Babul 2005a,b; Benson 2005; Gao et al 2004; Diemand et al 2007a,b).

Consensus has been slowly but steadily emerging on these issues. For example, the *mass function* of subhalos has been found to be rather steep, $dN/dM \propto M_{\text{sub}}^{-1.8}$ or steeper, implying that the subhalo population is dominated in number by low-mass systems but that most of the substructure mass resides with the few most massive subhalos (Springel et al 2001, Helmi, White & Springel 2002, Gao et al 2004). Confirmation for this comes from the fact that the total fraction of mass in subhalos has remained rather low (typically below 10%) even in the highest resolution simulations published so far (although see Diemand et al 2007a,b for a differing view).

Subhalos have also been found to be *spatially biased* relative to the smooth dark matter halo where they are embedded, avoiding in general the innermost regions. Furthermore, the number density profile of the subhalo population also differs markedly from that of galaxies in clusters. This precludes identifying directly the population of “surviving” subhalos with galaxies within clusters, and highlights the need for either more sophisticated numerical modeling techniques, or for pairing up

⁶ Email: ludlow@uvic.ca

the N-body results with semi-analytic modeling in order to trace more faithfully the galaxy population (Springel et al 2001, De Lucia et al 2004, Gao et al 2004).

Kinematically, the bias in the spatial distribution of subhalos relative to the dark matter is reflected as a mild velocity dispersion bias. Diemand et al (2004), for example, find $\sigma_{\text{sub}}/\sigma_{\text{DM}} \sim 1.12 \pm 0.04$, and report that the velocity distribution of subhalos resembles that of the dark matter, with a weak radial anisotropy that increases with radius.

One intriguing result of all these studies has been the remarkably weak dependence of the properties of substructure on subhalo mass. Gao et al (2004) and Diemand, Moore & Stadel (2004), for example, find that the radial distribution of subhalos is largely independent of their self-bound mass. This is surprising given the strong mass dependence expected for the processes that dictate the evolution of subhalos within the main halo, such as dynamical friction and tidal stripping. Although efficient mixing within the potential of the main halo is a possibility, an alternative explanation has been advanced by Kravtsov, Gnedin & Klypin (2004).

These authors argue that the *present-day* mass of a subhalo may be a poor indicator of the *original* mass of the system, which may have been substantially larger at the time of accretion, and used this idea to motivate how the faintest dwarf companions of the Milky Way were able to build up a sizable stellar mass through several episodes of star formation despite their shallow present-day potential wells. The same idea was also adopted by Libeskind et al (2007) as a possible reason for the peculiar spatial alignment of satellites around the Milky Way (Lynden-Bell 1976, 1982; Kunkel & Demers 1976; Kroupa, Thies & Boily 2005).

We revisit here these issues with the aid of a suite of high-resolution N-body simulations of galaxy-sized halos. We extend prior work by carefully tracking the orbits of the surviving subhalos back in time. This allows us to select a complete set of subhalos *physically associated* with the main halo, rather than only the ones that happen to be within the virial radius at a particular time. As we discuss below, a large fraction of the associated subhalo population are on unorthodox orbits that take them well beyond the virial radius, a result with important implications for studies of satellite galaxies and of halos clustered around massive systems.

The plan of this paper is as follows. We introduce briefly the numerical simulations in § 2 and describe our subhalo detection algorithm and tracking method in § 3. Our main results are presented in § 4: we begin by exploring the subhalo spatial distribution and kinematics, as well as their dependence on mass, and discuss the consequences of our findings for the subhalo mass function. We end with a brief summary and discussion of possible implications and future work in § 5.

2. THE NUMERICAL SIMULATIONS

2.1. The Cosmological Model

All simulations reported here adopt the concordance Λ CDM model, with parameters chosen to match the combined analysis of the first-year WMAP data release (Spergel et al 2003) and the 2dF Galaxy Redshift Survey (Colless et al 2001). The chosen cosmological parameters are $\Omega_{\text{m}} = \Omega_{\text{dm}} + \Omega_{\text{b}} = 0.25$, $\Omega_{\text{b}} = 0.045$,

$h = 0.73$, $\Omega_{\Lambda} = 0.75$, $n = 1$, and $\sigma_8 = 0.9$. Here Ω denotes the present-day contribution of each component to the matter-energy density of the Universe, expressed in units of the critical density for closure, $\rho_{\text{crit}} = 3H^2/8\pi G$; n is the spectral index of the primordial density fluctuations, and σ_8 is the rms linear mass fluctuation in a sphere of radius $8 h^{-1}$ Mpc at $z = 0$. Hubble’s “constant” is given by $H(z)$ and parameterized at $z = 0$ by $H(z = 0) = H_0 = 100 h \text{ km s}^{-1} \text{ Mpc}^{-1}$.

2.2. The Runs

Our analysis is based on a suite of 5 high-resolution simulations of the formation of galaxy-sized Λ CDM halos. The simulations target halos of virial mass², $M_{200} \sim 10^{12} h^{-1} M_{\odot}$, and have at $z = 0$ between 3 and 5 million particles within the virial radius, r_{200} . Each halo was selected at random from a list of candidates compiled from a cosmological N-body simulation of a large ($100 h^{-1}$ Mpc) periodic box and resimulated individually at higher resolution using the technique described in detail by Power et al (2003). We imposed a mild isolation criterion (that no neighbors with mass exceeding $5 \times 10^{11} h^{-1} M_{\odot}$ be found within $1 h^{-1}$ Mpc at $z = 0$) in order to exclude systems formed in the periphery of much larger groups or clusters.

The simulations were run with **Gadget2**, a massively-parallel cosmological N-body code (Springel 2005). Particle pairwise interactions were softened using the “optimal” gravitational softening length scale suggested by Power et al (2003); i.e., a spline lengthscale $h_s = 1.4 \epsilon_G \approx 4 r_{200}/\sqrt{N_{200}}$, kept fixed in comoving coordinates. Numerical details of each run are listed in Table 1.

3. THE ANALYSIS

3.1. Substructure Finding

We use **SUBFIND** (Springel et al 2001) in order to identify self-bound structures in N-body simulations. **SUBFIND** finds substructure within friends-of-friends (FOF, Davis et al 1985) halos by locating overdense regions within each FOF halo and identifying the bound subset of particles associated with each overdensity. **SUBFIND** also works recursively and its output readily identifies “subhalos within subhalos”, thus characterizing fully the various levels of the hierarchy of substructure present within a given FOF halo. We retain for our catalogue all **SUBFIND** subhalos with more than 20 particles.

The main output of **SUBFIND** is a list of subhalos within each FOF halo, together with their structural properties. For the purposes of this paper, we shall focus on: (i) the subhalo self-bound mass, M_{sub} ; (ii) the peak of its circular velocity profile (characterized by r_{max} and V_{max}); and (iii) the position of the subhalo center, which we identify with the particle with minimum gravitational poten-

² We define the virial mass of a halo, M_{200} , as that contained within a sphere of mean density $200 \times \rho_{\text{crit}}$. The virial mass defines implicitly the virial radius, r_{200} , and virial velocity, $V_{200} = \sqrt{GM_{200}/r_{200}}$, of a halo, respectively. We note that other definitions of “virial radius” have been used in the literature; the most popular of the alternatives adopts a density contrast (relative to critical) of $\Delta \approx 178 \Omega_{\text{m}}^{0.45} \sim 100$ (for our adopted cosmological parameters, see Eke et al 1996). We shall refer to these alternative choices, where appropriate, with a subscript indicating the value of Δ ; i.e., r_{100} is the virial radius obtained assuming $\Delta = 100$.

tial energy. We have run SUBFIND on all 100 snapshots (equally spaced in scale factor, a , of each of our runs, and are therefore able to track in detail the evolution of individual subsystems and their particle members.

3.2. Substructure Tracking

Our analysis focuses on all *surviving* subhalos at $z = 0$ and relies heavily on tracking accurately their accretion history. To this aim, we trace each subhalo backwards in time by identifying the central particle at $z = 0$ and searching for the group it belongs to in the immediately preceding snapshot. A new central particle is then selected and the procedure is iterated backwards in time until $z = 9$, the earliest time we consider in the analysis.

This procedure leads in general to a well-defined evolutionary track for each subhalo identified at $z = 0$. When no subhalo is found to contain a subhalo’s central particle in the immediately preceding snapshot, the search is continued at earlier times until either a progenitor subhalo is found or $z = 9$ is reached. This is necessary because a subhalo may temporarily disappear from the catalogue, typically at times when it falls below the minimum particle number or else when it is passing close to the center of a more massive system and its density contrast is too low to be recognized by SUBFIND. Our procedure overcomes this difficulty and in most cases recovers the subhalo at an earlier time. We note that these complications are a fairly common occurrence in the analysis procedure, and we have gone to great lengths to make sure that these instances are properly identified and dealt with when constructing our subhalo catalogue and their accretion histories.

The tracking procedure described above defines a unique trajectory for each subhalo identified at $z = 0$. This trajectory may be used to verify whether a subhalo has, at any time in the past, been accreted within the (evolving) virial radius of the main halo. If this is the case, we record the time it first crosses $r_{200}(z)$ as the “accretion redshift”, z_{acc} , and label the subhalo as *associated* with the main system³. On the other hand, halos that have *never* been inside the virial radius of the main halo will be referred to as “field” or “infalling” halos.

Using the subhalo trajectories, we compute and record a few further quantities of interest for each subhalo; namely,

- its “turnaround” distance, r_{ta} , defined as the *maximum separation* between a subhalo and the center of the main progenitor before $z = z_{\text{acc}}$ (for associated subhalos) or $z = 0$ (for field subhalos);
- the structural properties of associated subhalos at accretion time, such as mass and peak circular velocity;
- an apocentric distance, r_{apo} , defined as the apocenter of its orbit computed at $z = 0$ using the subhalo’s instantaneous kinetic energy and orbital angular momentum, together with the potential of

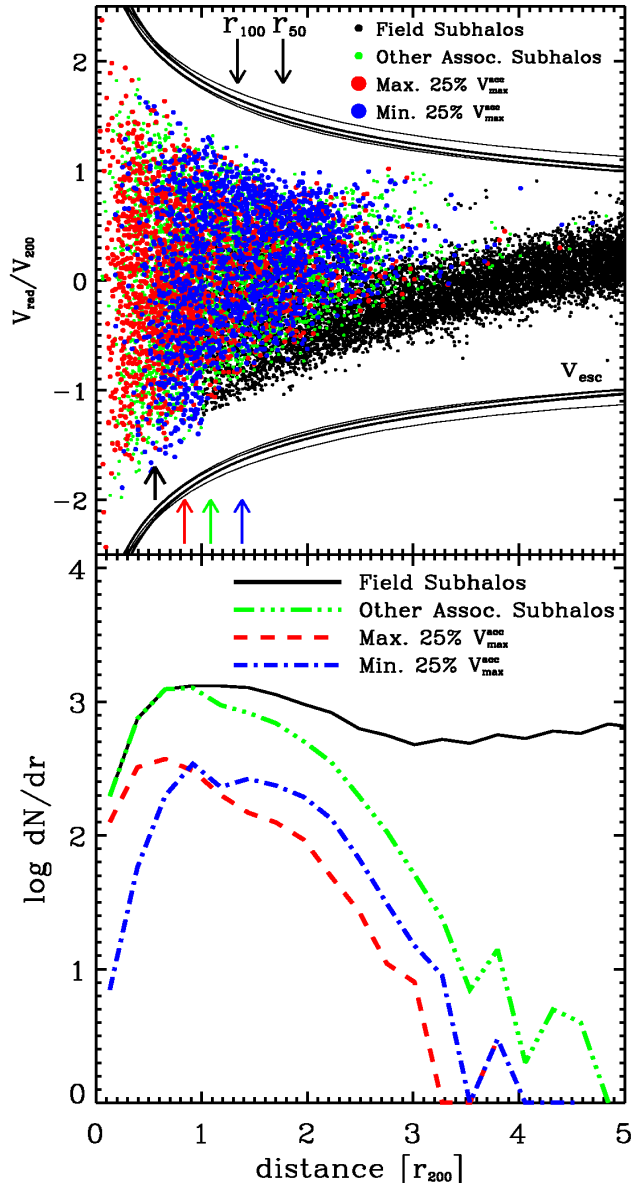


FIG. 1.— *Upper panel*: Radial velocity versus distance to the main halo center for all subhalos within $5 \times r_{200}$ in our simulations. Velocities and distances are normalized to the virial velocity, V_{200} , and virial radius, r_{200} , of each host. All “associated” halos are shown in color, subhalos on first infall are shown in black. Different colors are used according to the peak circular velocity of the subhalo at the time of accretion. Blue denotes the quartile with smallest $V_{\text{max}}^{\text{acc}}$, red to those with largest $V_{\text{max}}^{\text{acc}}$. Green denotes the rest of the associated subhalo population. Upward vertical arrows indicate the half-number radius for the various subhalo populations. A shorter black arrow marks the half-number radius for “associated” dark matter particles. We find that 65% of subhalos in the range $r_{200} < r < 2r_{200}$ are actually “associated” and have thus already been within the host virial radius in the past. Roughly one third of subhalos between $2r_{200} < r < 3r_{200}$ are also physically “associated” with the main halo. The upper and lower bounding curves denote the escape velocity for each of the five simulated halos. *Lower panel*: Radial distribution of subhalos. Color key is the same as in the upper panel.

³ Analogously, we identify a set of *associated dark matter* particles by compiling a list of all particles that were at some time within the virial radius of the main halo but are not attached to any substructure at $z = 0$.

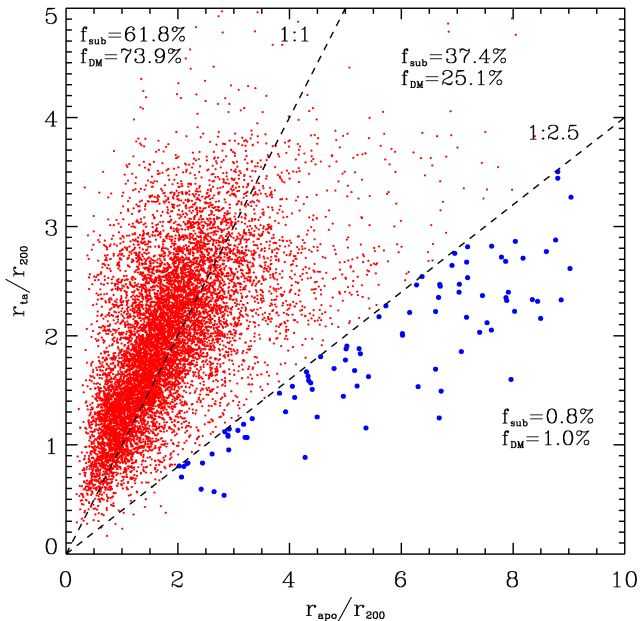


FIG. 2.— Turnaround radius versus apocentric distance at $z = 0$ for all *associated* subhalos in our simulations. The turnaround distance is the maximum distance from the main halo before accretion. Subhalos on “traditional” orbits are expected to have $r_{\text{apo}} < r_{\text{ta}}$ and, thus, to be to the left of the 1:1 curve in this plot. Subhalos near the 1:1 line have $r_{\text{apo}} \approx r_{\text{ta}}$ and are therefore on orbits which have not been decelerated substantially since turnaround. Subhalos with $r_{\text{apo}} > r_{\text{ta}}$ are on unorthodox orbits and they have *gained* orbital energy during or after accretion. The blue symbols in the panel highlight subhalos on extreme orbits, that will take them more than ~ 2.5 times farther than their turnaround radius. The fraction of associated subhalos and associated dark matter particles in each region of the plot is given in the legends.

the main halo⁴.

Subhalo quantities measured at accretion time will be referred to by using the sub/superscript “acc”; for example, $V_{\text{max}}^{\text{acc}}$ refers to the peak circular velocity of a subhalo at $z = z_{\text{acc}}$. Quantities quoted without superscript are assumed to be measured at $z = 0$ unless otherwise specified; e.g., $V_{\text{max}} = V_{\text{max}}(z = 0)$.

4. RESULTS

The basic properties of our simulated halos at $z = 0$ are presented in Table 1. Here, $\epsilon_G (= h_s/1.4)$ is the **Gadget** gravitational softening scalelength, and M_{200} , r_{200} , and N_{200} are, respectively, the halo virial mass, radius, and number of particles within r_{200} . Table 1 also lists the peak of the circular velocity of the main halo, V_{max} , and its location, r_{max} ; the total number of “associated” subhalos; as well as the number of those found within various characteristic radii at $z = 0$.

4.1. Subhalos beyond the virial radius

One surprise in Table 1 is that the number of “associated” subhalos exceeds by about a factor of ~ 2 the total number of subhalos identified within r_{200} . This result is also illustrated in Fig. 1, where we show, at $z = 0$,

⁴ For simplicity, we use the potential of an NFW profile fitted to the inner mass profile of the halo, but our conclusions are insensitive to this simplification.

the distance from the main halo center vs radial velocity for all subhalos identified in our simulations. Distances and velocities have been scaled to the virial quantities of each primary halo. Colored dots are used to denote “associated” subhalos, black symbols for “field” halos. Different colors correspond to different subhalo masses, as measured by the peak circular velocity at accretion time (in units of the present-day primary halo virial velocity, V_{200}): red is used for subhalos with $V_{\text{max}}^{\text{acc}} \geq 0.72 V_{200}$, blue for those with $V_{\text{max}}^{\text{acc}} \leq 0.038 V_{200}$, green for the rest.

Note that the distribution of associated subhalos extends well past $\sim 3 r_{200}$; indeed, a few associated subsystems are found at $r \sim 4 r_{200}$ moving outwards with radial velocity of order $V_r \sim V_{200}$. A careful search shows that there are actually several associated subhalos presently at distances larger than $\sim 5 r_{200}$.

This result is unexpected in simple formation scenarios, such as the *spherical secondary infall model* (SSIM, for short). SSIM identifies at any time three distinct regions around a halo: (i) an inner “virialized” region where accreted mass shells have had time to cross their orbital paths; (ii) a surrounding “first infall” region, where shells are still on first approach and have not yet crossed; and (iii) a still expanding outer envelope beyond the current turnaround radius (Bertschinger 1985, White et al 1993, Navarro & White 1993). The boundary of the virialized region is roughly delineated by the virial radius (hence its name), and the turnaround occurs just outside $\sim 3 r_{200}$.

Thus, according to the SSIM, few, if any, associated subhalos are expected to populate the region outside r_{200} . This is clearly at odds with the results shown in Fig. 1 and Table 1: more than *half* of all associated subhalos are found beyond r_{200} at $z = 0$! This conclusion is insensitive to our particular definition of the virial radius; revising our definition from a density contrast of 200 to 100 does not change matters much. As shown in Fig. 1, r_{100} is on average only $\sim 30\%$ larger than r_{200} so that still about one in three associated subhalos lie beyond r_{100} .

4.2. The orbits of associated subhalos

The discrepancy between the simulation results and the naive expectation of the SSIM was pointed out by Balogh, Navarro & Morris (2000), and confirmed by subsequent studies (Mamon et al 2004, Gill et al 2005, Diemand et al 2007) but its physical origin has not yet been conclusively pinned down. One of the premises of the secondary infall model is that the energy of a mass shell accreted into the halo is gradually reduced after its first pericentric passage until it reaches equilibrium. During this process, the apocentric distance of the shell is constantly reduced; for example, taking as a guide the SSIM self-similar solutions of Bertschinger (1985), the *second* apocenter of an accreted shell (the first would be its “turnaround” radius) is roughly 90% of its turnaround distance, r_{ta} , and the shell gradually settles to equilibrium, approaching a periodic orbit with $r_{\text{apo}} \sim 0.8 r_{\text{ta}}$.

Associated subhalos found today outside the virial radius have clearly evolved differently from this prescription, and it is instructive to study the way in which the difference arises. One possibility is that deviations from spherical symmetry during accretion might be responsible for the outlying associated subhalos. Accretion through the filamentary structure of the cosmic web sur-

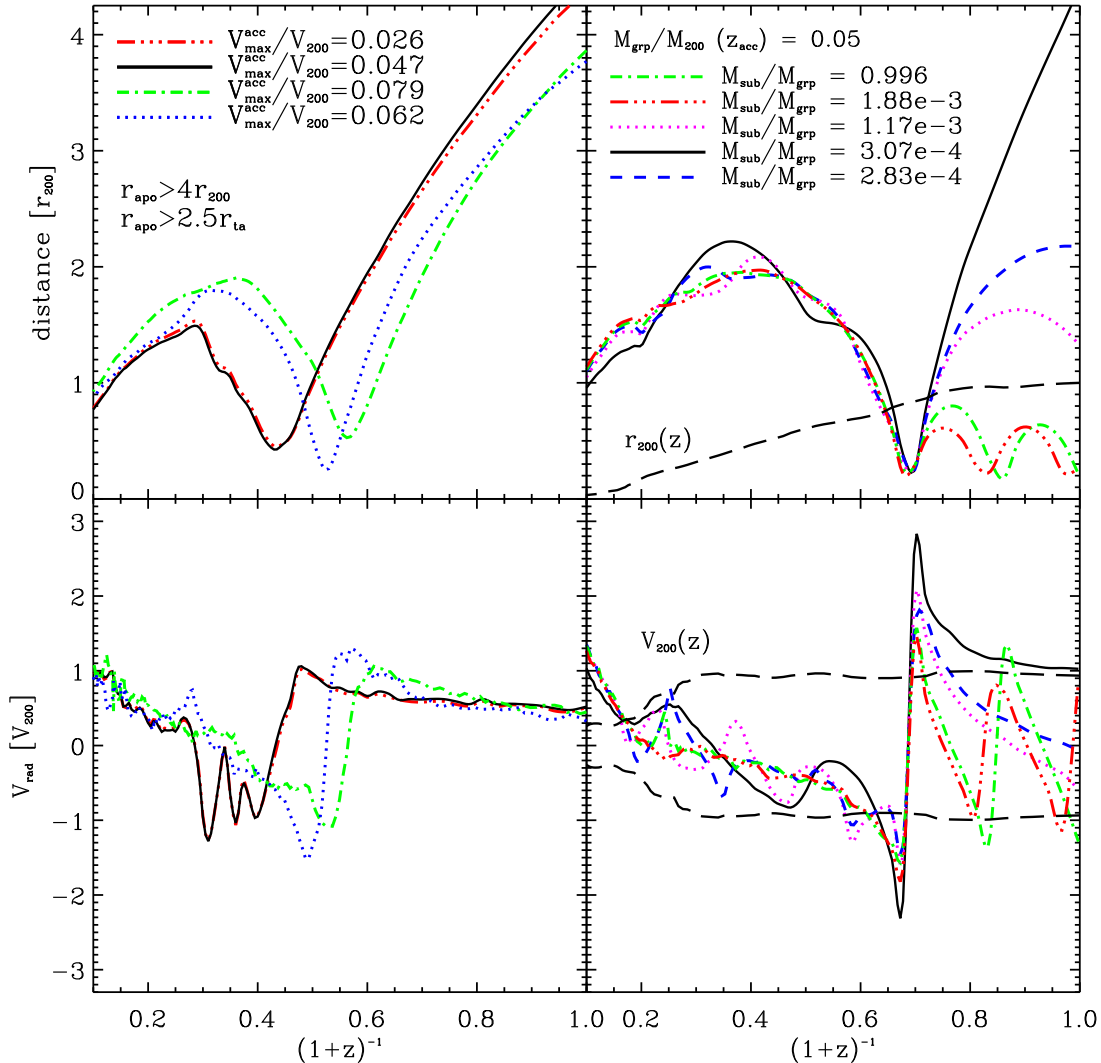


FIG. 3.— Orbital trajectories of selected subhalos. Upper panels show the distance to the center of the main progenitor as a function of expansion factor. The top-left panel shows the trajectories of 4 subhalos on “extreme” orbits (i.e., $r_{\text{apo}} > 2.5r_{\text{ta}}$; blue points in Fig. 2). Note that all of these systems gain energy during their first pericentric approach to the main halo. The top-right panel illustrates that multiple-body interactions occurring during the tidal dissociation of bound groups of subhalos is responsible for propelling some satellites onto extreme orbits. At pericentric approach, the tidal field of the main halo breaks apart the group, and redistributes each member onto orbits of varying energy. The most affected are, on average, the least massive members of the group, some of which are pushed onto orbits with extremely large apocenters. The dashed curve shows the growth of the virial radius of the most massive progenitor of the main halo. Bottom panels show the radial velocity of the subhalos shown in the upper panels.

rounding the halo, for example, might result in a number of subhalos on orbits of large impact parameter that simply “graze” the main halo and are therefore not decelerated during their first pericentric approach, as assumed in the secondary infall model. These subhalos would lose little orbital energy, and should presumably be today on orbits with apocentric distances of the order of their original turnaround radii. According to the analytic calculation of Mamon et al (2004), systems on such orbits may reach distances as far as $r_{\text{apo}} \sim 2.3r_{200}$.

We explore this in Fig. 2, where we show the turnaround radius of each associated subhalo versus their apocentric distance estimated at $z = 0$, both normalized to the virial radius of the main halo. Subhalos that have

followed the traditional orbits expected from the SSIM should lie to the left of the 1:1 curve in this panel. These, indeed, make up the bulk ($\sim 62\%$) of the associated population.

Note as well that there are a number of subhalos near the 1:1 line, whose orbits have not been decelerated since accretion into the main halo. These are objects that are either on their way to first pericentric passage or, as discussed in the above paragraph, that have somehow evaded significant breaking during accretion.

More intriguingly, Fig. 2 also shows that there are a significant number of subhalos on decidedly unorthodox orbits, with apocenters exceeding their SSIM theoretical “maximum”; i.e., $r_{\text{apo}} > r_{\text{ta}}$. Indeed, $\sim 38\%$ of associ-

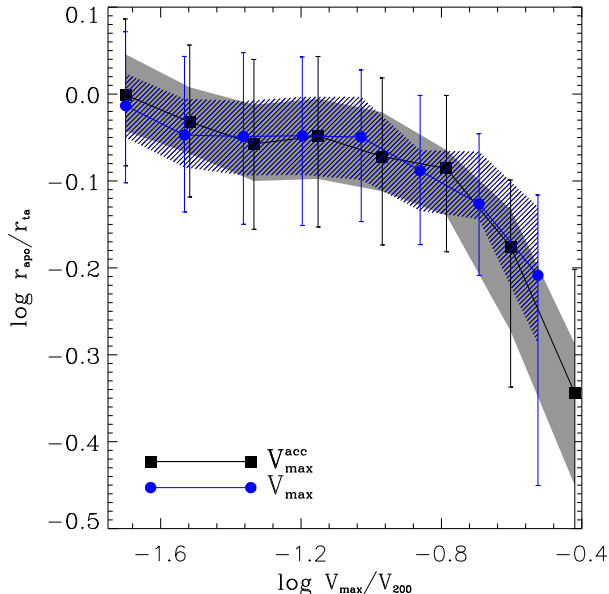


FIG. 4.— The ratio of apocentric radius (estimated at $z = 0$) to turnaround distance as a function of the peak circular velocity, V_{\max} , of a subhalo. Two estimates of V_{\max} are used for each subhalo, one measured at accretion time and another at $z = 0$. Symbols correspond to the median of the distribution, shaded areas encompass 25% of the distribution around the median, and the extremes of the error bars correspond to the 25th and 75th centiles. Note that only fairly massive associated subhalos are today on orbits substantially more bound than when they turned around. The median apocentric radius of low-mass subhalos is of order of the virial radius, indicating that about *half* of all associated subhalos spend a substantial fraction of their orbital period outside r_{200} . Note that the effect depends only weakly on V_{\max} below a certain threshold; this presumably indicates that, below a certain mass limit, subhalos behave like test particles in the potential of the main halo.

ated subhalos are on such orbits, and about $\sim 1\%$ are on orbits so extreme that their apocenters exceed their original turnaround distance by more than a factor of ~ 2.5 (the latter are highlighted in blue in Fig. 2). The large fraction of systems in such peculiar orbits, where the subhalo has *gained* orbital energy since turnaround, indicates that deviations from spherical symmetry play a minor role in pushing subhalos beyond r_{200} , and suggests that another mechanism is at work.

4.3. Subhalo mass dependence of unorthodox orbits

One clue to the mechanism able to push some subhalos onto highly energetic orbits is the strong dependence of the effect on the mass of the subhalo. This is illustrated in the bottom panel of Fig. 1, which shows that low-mass subhalos are the ones being preferentially pushed to the outskirts of the halo.

Further clues result from inspecting individually the trajectories of some of the subhalos on extreme orbits. This is shown in the top-left panel of Fig. 3, where we show the orbits of a few of the associated subhalos with $r_{\text{apo}} > 2.5 r_{\text{ta}}$. Interestingly, all of these subhalos have very low mass at accretion ($V_{\max}^{\text{acc}} \lesssim 0.08 V_{200}$) and seem to acquire their “boost” in orbital energy during their first pericentric passage.

The “wiggles” in their trajectories prior to pericenter betray the fact that they actually belong to a bound system of multiple subhalos accreted as a single unit (Sales et al 2007a, Li & Helmi 2007). This is shown more clearly in the top-right panel of Fig. 3, where we show the trajectories of 5 subhalos belonging to one such group. The mass of the group is concentrated in the most massive member (see legends in the figure), which is surrounded (prior to accretion) by 4 bound satellites. The group contributes about 5% of the main halo’s mass at accretion time, $a_{\text{acc}} = (1 + z_{\text{acc}})^{-1} \approx 0.65$. The group as a whole turns around at $a_{\text{ta}} \approx 0.35$ and accretes on a $(r_{\text{per}}:r_{\text{apo}}) = (1:10)$ orbit that reaches $r_{\text{per}} \sim 0.25 r_{200}$ at $a_{\text{per}} \sim 0.69$.

During pericentric passage, the group is dissociated by the tidal field of the main halo, and its 5 members are flung onto orbits of widely different energy. The most massive object (single dot-dashed curve in the right panels of Fig. 3) follows a “traditional” orbit, rebounding to a second apocenter which is only $\sim 30\%$ of its turnaround distance. The rest evolve differently; the least massive subhalos, in particular, tend to *gain* energy during the disruption of the group and recede to a second apocenter well outside the original turnaround. As anticipated by the work of Sales et al (2007b) this is clearly the result of multiple-body interactions occurring during the first pericentric passage of the group.

This is confirmed by the bottom panels in Fig. 3, which show the evolution of the radial velocity of each subhalo. The least massive member of the group is, in this case, the least bound as well, judging from its excursions about the group’s center of mass. This subhalo (solid black line in the right panels of Fig. 3) happens to be approaching the group’s orbital pericenter at about the same time when the group as a whole approaches the pericenter of its orbit. This coincidence in orbital phase allows the subhalo to draw energy from the multiple-body interaction; the subhalo is thus propelled onto an orbit that will take it beyond three times its turnaround distance, or $\sim 6 r_{200}$. Although technically still bound, for all practical purposes this subhalo has been physically ejected from the system and might be easily confused for a system that has evolved in isolation.

The ejection process is reminiscent of the findings of early N-body simulations, which showed that the ejection of a small but sizable fraction of particles is a general result of the violent potential fluctuations that accompany the collapse of a dynamically cold N-body system (see, e.g., van Albada 1982). These occur as small inhomogeneities are amplified by the collapse, allowing for substantial energy transfer between particles as the inhomogeneities are erased during the virialization of the system.

It is important to point out that not all low-mass subhalos are affected equally. For example, despite being of comparable mass to the ejected object, one of the low mass members of the group ends up on an orbit almost as tightly bound as the main subhalo (red triple dot-dashed curve in Fig. 3). This shows that the orbital fate of a subhalo is mainly determined by its orbital phase within the accreting group at the time of accretion. Depending on this, subhalos may either *lose* or *gain* orbital

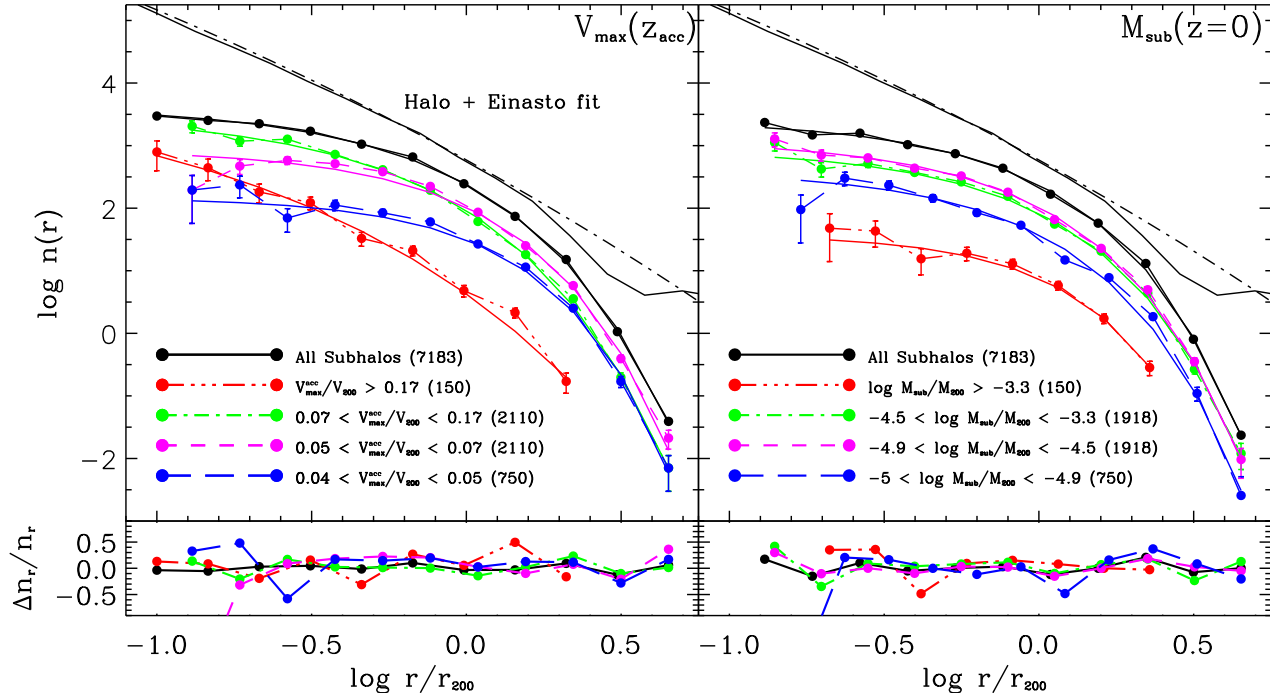


FIG. 5.— Number density profile of associated subhalos, after stacking the results of all 5 simulations in our series. The black solid symbols show the result for all subhalos, the other symbols correspond to various subsamples obtained after splitting by either V_{\max}^{acc} (left panel) or by subhalo mass at $z=0$ (right-hand panel). Solid lines through each curve correspond to the best fits obtained with eq. 1. The parameters of each fit are listed in Table 2. Lines without symbols show the dark matter density profile. Note that the spatial distribution of subhalos depends sensitively on subhalo mass when measured by V_{\max}^{acc} , but that, in agreement with prior work, the mass bias essentially disappears when adopting M_{sub} to split the sample. See text for further discussion.

energy during the interaction.⁵

Despite this apparent symmetry, it is clear that low mass halos are preferentially “ejected” or placed on high-energy orbits through this process. This enhances their survival probability by placing them on orbits where they spend extended periods in the periphery of the main halo, outside the region where tidal fields may effectively strip and disrupt them.

The combination of these two effects (energy gain and enhanced survival likelihood) leads to a strong mass dependence on the orbital properties of associated subhalos at $z=0$. This is illustrated in Fig. 4, where we show the ratio of apocenter (estimated at $z=0$) to turnaround distance as a function of subhalo peak circular velocity. This figure shows clearly that the most massive subhalos are found today in orbits with apocentric distances much smaller than their turnaround: halos with $V_{\max}^{\text{acc}} \sim 0.4 V_{200}$ (which corresponds to roughly $M_{\text{sub}}^{\text{acc}} \sim 0.1 M_{200}$) have median apocenters of order half their turnaround distance. On the other hand, the median apocenter of associated subhalos with $V_{\max}^{\text{acc}} \lesssim 0.1 V_{200}$ is of the order of the turnaround radius.

Note as well that the V_{\max} dependence is quite pronounced at the high-mass end but rather weak for low-mass subhalos. This presumably reflects the fact that,

⁵ This is analogous to the mechanism responsible for the creation of *two* “tidal tails” in merging N-body systems (Toomre & Toomre 1972), consisting, respectively, of particles which either *lose* or *gain* orbital energy during the interaction.

once a subhalo is small enough, it behaves more or less like a test particle in the potential of the main system.

Finally, note that the mass dependence is less pronounced when the *present-day* subhalo V_{\max} is used. This is because tidal stripping has a more pronounced effect on systems that orbit nearer the center of the main halo. The more massive the subhalo at accretion the closer to the center it is drawn and the more substantial its mass loss, weakening the mass-dependent bias illustrated in Fig. 4. We shall see below that the mass dependence becomes even weaker when expressed in terms of the *present-day* subhalo mass.

4.4. Subhalo spatial distribution

The number density profile of all associated subhalos is shown by the top (black) symbols in Fig. 5. The profile may be approximated rather accurately by the same empirical formula introduced by Navarro et al (2004) to describe the mass profile of CDM halos. This profile is characterized by a power-law dependence on radius of the logarithmic slope of the density, $d \log \rho / d \log r \propto r^{-\alpha}$, which implies a density profile of the form,

$$\ln(n(r)/n_{-2}) = -(2/\alpha)[(r/r_{-2})^\alpha - 1]. \quad (1)$$

This density law was first introduced by Einasto (1965), who used it to describe the distribution of old stars within the Milky Way. For convenience, we will refer to it as the Einasto profile. The scaling parameters n_{-2} and r_{-2} may also be expressed in terms of the *central*

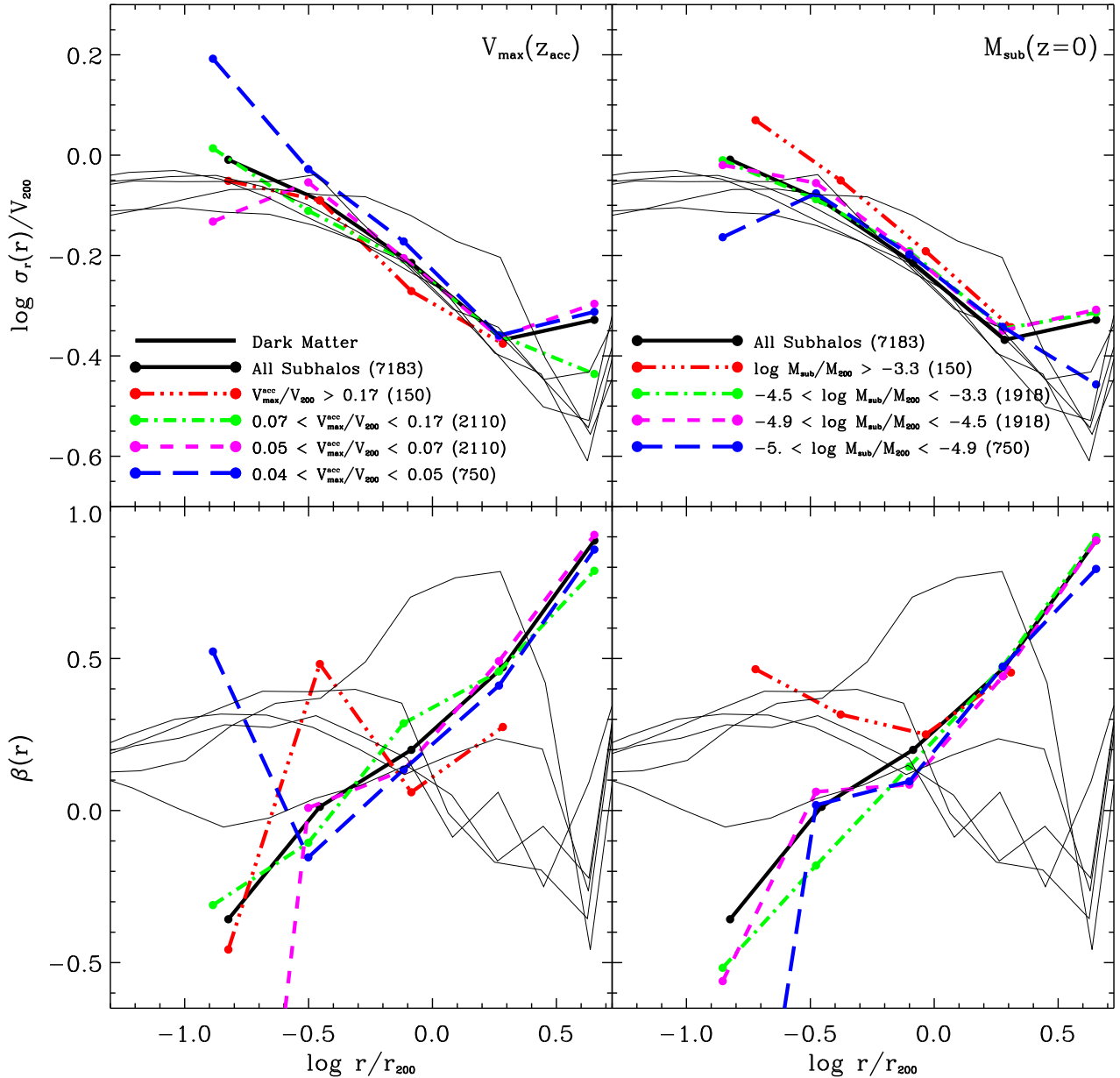


FIG. 6.— Radial velocity dispersion and anisotropy profiles for dark matter (thin black lines) and associated subhalos (thick colored lines). Symbols are described in the legend and are the same as in Fig. 5. Note that the mass-dependent bias shown in Fig. 5 is also reflected in the subhalo kinematics: low mass subhalos tend to have higher velocity dispersions than their high-mass counterparts. This bias is clearer when measuring subhalo mass by the peak circular velocity at accretion time, V_{\max}^{acc} , rather than by the self-bound mass at $z=0$, M_{sub} . Note as well that subhalos tend to be on orbits less radially biased than the dark matter, especially near the center. This is presumably because subhalos on tangentially-biased orbits avoid the innermost regions of the main halo, thus enhancing their survival probability.

value of the profile, $n_0 = n(r=0) = \exp(2/\alpha) n_{-2}$, and by the radius containing *half* of the associated subhalos, r_h .

We list in Table 2 the parameters obtained by fitting eq. 1 to the subhalo number density profiles. (Note that the units used for n_0 are arbitrary, but they are consistent, in a relative sense, for the various subhalo popula-

tions.) As discussed by Navarro et al (2004), Merritt et al (2005, 2006), and more recently by Gao et al (2007), Λ CDM halo density profiles are well described by α_{DM} in the range ~ 0.15 - 0.3 . This is in sharp contrast with the much larger values obtained for the subhalo number density profile ($\alpha_{\text{sub}} \sim 1.0$; i.e., the 3D radial distribution of subhalos is approximately “exponential”), and quanti-

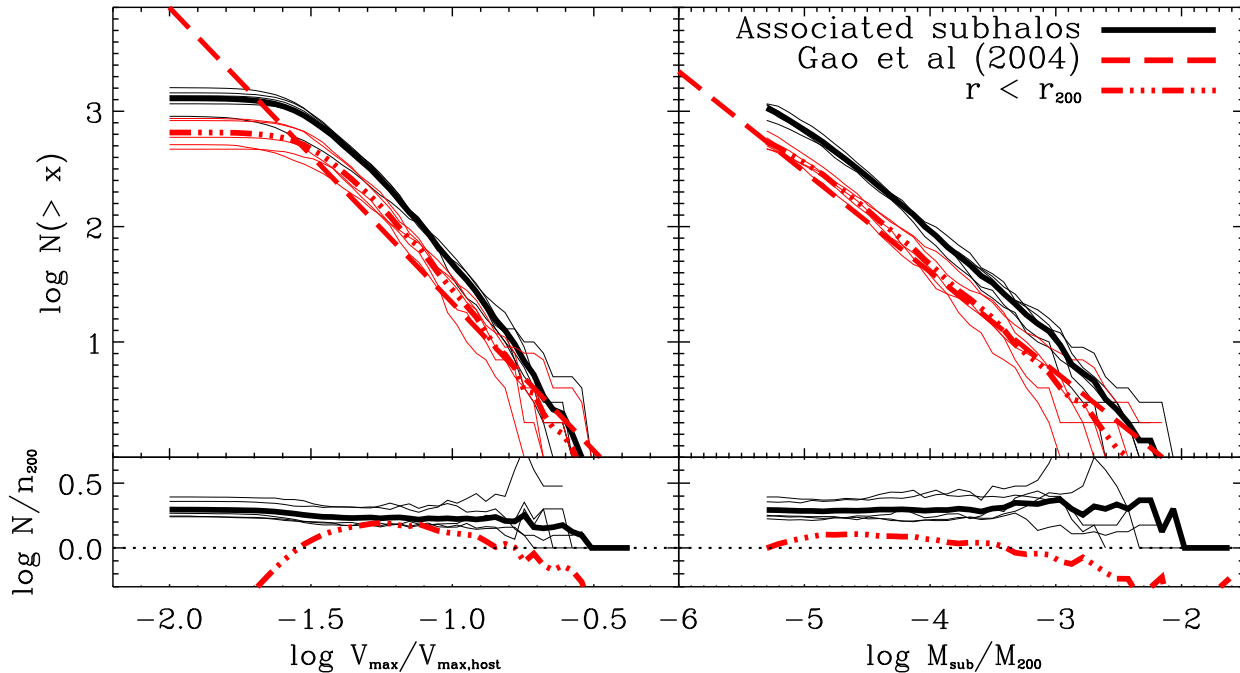


FIG. 7.— Associated subhalo mass (M_{sub}) and peak circular velocity (V_{max}) cumulative distributions (both quantities measured at $z = 0$). Black lines correspond to all associated subhalos; red lines to subhalos identified within r_{200} . Thick lines in each panel denote the average of our 5 simulations. Note that the number of associated subhalos exceeds by about a factor of ~ 2 the number of subhalos found within r_{200} . The residuals are computed relative to the subhalo population within the virial radius. Our results agree well with those of Gao et al (2004), shown by the thick dashed lines as simple power-law fits: $\log_{10} N(> V_{\text{max}}) = -2.559 \log_{10}(V_{\text{max}}/V_{\text{max}}^{\text{host}}) - 1.221$, and $\log_{10} N(> M_{\text{sub}}) = -0.869 \log_{10}(M_{\text{sub}}/M_{200}) - 1.869$, respectively.

fies the well-established spatial bias between the subhalo population and the dark mass profile of the main halo.

As mentioned in Sec. 1, the larger values of α characterizing the subhalo spatial distribution imply a large nearly constant density “core” in their profile, in contrast with the “cuspy” density profile of the dark halo, shown as a solid line (without symbols) in Fig. 5.

The left panel in Fig. 5 shows that the subhalo spatial distribution depends sensitively on subhalo mass, as measured by the peak circular velocity at accretion, $V_{\text{max}}^{\text{acc}}$. The various colored profiles in this panel correspond to splitting the sample of subhalos in four groups, according to the value of $V_{\text{max}}^{\text{acc}}$ (normalized to V_{200} , the virial velocity of the main halo at $z = 0$). The concentration increases systematically with $V_{\text{max}}^{\text{acc}}$; for example, half of the ~ 150 (surviving) subhalos with $V_{\text{max}}^{\text{acc}} > 0.17V_{200}$ are contained within $\sim 0.7r_{200}$ at $z = 0$. The corresponding radius for subhalos with $0.04 < V_{\text{max}}^{\text{acc}}/V_{200} < 0.05$ is $\sim 1.1r_{200}$ (see details in Table 2).

Interestingly, the mass dependence of the subhalo number density profile essentially disappears when the *present-day* subhalo mass is used to split the sample. This is illustrated in the right-hand panels of Fig. 5, which shows that the shape of the density profile of subhalos differing by up to two decades in mass is basically the *same*. This is in agreement with the earlier results of Gao et al (2004) and Diemand et al (2004), but indicates that the apparent mass-independence of the subhalo spatial distribution is *not* the result of efficient mixing within the main halo, but rather a somewhat fortuitous result of the cancellation of the prevailing trend by dynamical

friction and tidal stripping.

It is conceivable that numerical artifact may also help to erase the dependence of $n_{\text{sub}}(r)$ on present-day subhalo mass. Indeed, SUBFIND (like every subhalo finder) will tend to assign masses to subhalos which depend slightly, but systematically, on their location within the main halo. The mass of subhalos near the center is more likely to be underestimated, and some subhalos may, indeed, be even missed altogether if close enough to the central cusp. Splitting the sample by $V_{\text{max}}^{\text{acc}}$ minimizes such effects and allows for the subhalo mass bias to be properly identified.

4.5. Velocity anisotropies

The mass dependence of the subhalo spatial distribution discussed in the previous subsection shows clearly in their kinematics, as shown in Fig. 6. The top panels of this figure show the radial velocity dispersion profile, $\sigma_r = \langle v_r^2 \rangle^{1/2}$, computed in spherical shells for the same subsamples discussed in Fig. 5. The bottom panels show the anisotropy profile, defined as $\beta \equiv 1 - (\sigma_\theta^2 + \sigma_\phi^2)/2\sigma_r^2$. The mean values of the velocity dispersion for each component are listed in Table 2.

The solid lines without symbols in Fig. 6 correspond to dark matter particles of the main halo, randomly sampled in order to match the total number of subhalos. As expected, the dark matter velocity distribution is mildly anisotropic, with a radial bias that increases outward and reaches a maximum near the virial radius.

The radial velocity dispersion profile of the subhalo population follows closely that of the dark matter, al-

though as a whole, the subhalo population is kinematically biased relative to the dark halo. The effect, however, is fairly weak; we find $\sigma_r^{\text{sub}}/\sigma_r^{\text{DM}} \sim 0.98$. There is evidence for a clear, albeit slight, dynamical bias in subsamples split according to $V_{\text{max}}^{\text{acc}}$. The velocity dispersion of the bin with $0.025 < V_{\text{max}}^{\text{acc}}/V_{200} < 0.04$ exceeds by a factor of 1.09 that of the most massive subsample, a result consistent with their relative spatial distributions (see details in Table 2).

As expected from the discussion in the previous subsection, the bias essentially disappears when splitting the subhalo population by the present-day mass of the subhalo, $M_{\text{sub}}(z=0)$. Within r_{200} , the velocity dispersion of subhalos with $4 \times 10^{-6} < M_{\text{sub}}/M_{200} < 8 \times 10^{-6}$ is actually comparable to that of halos in the largest mass bin ($M_{\text{sub}}/M_{200} > 5 \times 10^{-4}$, see Table 2).

Our results thus confirm the earlier conclusions of Ghigna et al (1998), Gao et al (2004), Diemand et al (2004) about the presence of a slight kinematic bias between subhalos and dark matter. Unlike the conclusions of Diemand et al, however, we find a significant discrepancy between the anisotropy profiles of the subhalo population and of the dark halo. As shown in the lower panels of Fig. 6, subhalos are on orbits less dominated by radial motions than the dark matter and, indeed, have a pronounced *tangential* bias near the center (i.e., for $r \lesssim 0.3 r_{200}$). With hindsight, this is not entirely unexpected, since subhalos nearer the center are more likely to survive if they are on tangentially-biased orbits that keep them away from the innermost regions of the halo, where tidal effects are strongest.

4.6. Subhalo mass function

The large number of associated subhalos on high-energy orbits discussed above imply that subhalos within the virial radius are just a fraction of all subhalos physically influenced by the main halo. This is illustrated quantitatively in Fig. 7, where we show the cumulative peak velocity and mass function of subhalos identified within r_{200} . The thin red lines in this figure correspond to subhalos identified within r_{200} ; black to the full sample of associated subhalos. Thick lines show the average results for the 5 simulated halos considered here. The residuals shown in the small panels are computed relative to the average for the associated subhalo population, and show that, on average, the total number of associated subhalos exceed those within r_{200} by a factor of ~ 2 . Our results within r_{200} are consistent with the work of Gao et al (2004), as indicated by the good agreement between the thick dot-dashed and dashed curves in Fig. 7.

Fig. 7 illustrates a number of interesting results. One is that, at the low mass end, the shape of the subhalo mass and velocity function is insensitive to the radius adopted for selection. Indeed, there is no obvious systematic trend with V_{max} or M_{sub} for $V_{\text{max}}/V_{\text{max}}^{\text{host}} \lesssim 0.2$. Below certain threshold, low mass subhalos behave as “test particles” in the potential of the main halo and their radial distribution becomes independent of mass. This implies that attempts to determine the asymptotic slope of the subhalo mass function are unlikely to be compromised by selecting for analysis only halos within the virial radius, as is traditionally done.

On the other hand, the subhalo mass function *shape* is substantially affected at the opposite end;

although about half of all associated subhalos with $V_{\text{max}} \lesssim 0.15 V_{\text{max}}^{\text{host}}$ are missing from within r_{200} , this fraction declines to one quarter for $V_{\text{max}} \sim 0.28 V_{\text{max}}^{\text{host}}$, and to zero for $V_{\text{max}} > 0.31 V_{\text{max}}^{\text{host}}$. As a result, in that mass range, the mass function of subhalos identified within r_{200} is shallower than that of associated systems. This may have interesting consequences for semianalytic modeling of the luminosity function in galaxy groups and clusters, which traditionally assume that all accreted subhalos remain within the virial radius of the main system.

5. SUMMARY AND DISCUSSION

We use a suite of cosmological N-body simulations to study the orbital properties of substructure halos (subhalos) in galaxy-sized cold dark matter halos. We extend prior work on the subject by considering the whole population of *associated* subhalos, defined as those that (i) survive as self-bound entities to $z=0$, and (ii) have at some time in the past been within the virial radius of the halo’s main progenitor. Our main findings may be summarized as follows.

- The population of *associated* subhalos extends well beyond three times the virial radius, r_{200} , and contains a number of objects on extreme orbits, including a few with velocities approaching the nominal escape speed from the system. These are typically the low-mass members of accreted groups which are propelled onto high energy orbits by multiple-body interactions during the tidal dissociation of the group in the potential of the main halo.
- The net result of this effect is to push low-mass subhalos to the periphery of the system, creating a well-defined mass-dependent bias in the spatial distribution of associated subhalos. For example, only about $\sim 29\%$ of subhalos which, at accretion time, had peak circular velocities of order 3% of the present-day virial velocity ($V_{\text{max}}^{\text{acc}} \sim 0.03 V_{200}$), are found today within r_{200} . This fraction climbs to $\sim 61\%$ and to $\sim 78\%$ for subhalos with $V_{\text{max}}^{\text{acc}} \sim 0.1 V_{200}$ and $\sim 0.3 V_{200}$, respectively.
- The strength of the bias is much weaker when expressed in terms of the subhalo *present-day* mass, presumably due to the increased effect of dynamical friction and tidal stripping on the most massive subsystems.
- The spatial distribution, kinematics, and velocity anisotropy of the subhalo population are distinct from the properties of the dark matter. Subhalos are less centrally concentrated, have a mild positive velocity bias, and are, near the center, on more tangential orbits than the dark matter.

The unorthodox orbits of substructure halos that result from the complex history of accretion in hierarchical formation scenarios have a number of interesting implications for theoretical and observational studies of substructure and of the general halo population.

One implication is that subhalos identified within the virial radius represent a rather incomplete census of the substructures physically related to (and affected by) a

massive halo. This affects, for example, the interpretation of galaxy properties in the periphery of galaxy clusters, and confirms earlier suggestions that evolutionary effects normally associated with passage through the innermost regions of a massive halo, such as tidal truncation or ram-pressure stripping, should be detectable well outside the traditional virial boundaries of a group or cluster (Balogh, Navarro & Norris 2000).

Furthermore, associated subhalos pushed well outside the virial radius of their main halo might be erroneously identified as separate, isolated structures in studies that do not follow in detail the orbital trajectories of each system. This effect would be most prevalent at low masses, and it is likely to have a significant effect on the internal properties of halos in the vicinity of massive systems. We expect, for example, halos in the periphery of groups/clusters to show evidence of truncation and stripping, such as higher concentrations and/or sharp cutoffs in their outer mass profiles.

The same effect may also introduce a substantial environmental dependence in the formation-time dependence of halo clustering reported in recent studies (Gao et al 2005; Zhu et al 2006; Jing et al 2007). In particular, at fixed mass, early collapsing halos might be more clustered because they are physically associated with a more massive system, from which they were expelled by multiple-body interactions.

A proposal along these lines has recently been advanced by Wang, Mo & Jing (2007), who argue that such environmental effects might be fully responsible for the age-dependence of halo clustering. Our physical interpretation, however, differs in detail from theirs. Whereas Wang et al argue for the suppression of mass accretion onto “old” halos by “heating by large-scale tidal fields” as responsible for their enhanced clustering, our results suggest that the real culprit is the orbital energy gain

associated with multiple-body interactions during accretion, which allows “old” low-mass halos to survive in the vicinity of massive systems until the present.

A further implication of our results concern the spatial bias of the most massive substructures discussed in S. 4.4. If, for example, luminous substructures in the Local Group trace the most massive associated subhalos at the time of accretion, they may actually be significantly more concentrated and kinematically biased relative to the dark matter, a result that ought to be taken into account when using satellite dynamics to place constraints on the mass of the halos of the Milky Way and M31.

Finally, as already pointed out by Sales et al (2007a,b), multiple-body interactions during accretion may also be responsible for the presence of dynamical outliers in the Local Group, such as Leo I and And XII. Further work is needed to assess whether the exceptional orbits of such systems could indeed have originated in the tidal dissociation of groups recently accreted into the Local Group. Since the latest proper motion studies of the Magellanic Clouds seem to suggest that the Clouds are on their first pericentric passage (Kallivayalil et al 2006; Piatek et al 2007), this is a possibility to consider seriously when trying to puzzle out the significance of the motion of the satellites of the Local Group.

We thank Simon White and Vincent Eke for useful discussions. ADL would like to thank Jorge Peñarrubia and Scott Chapman for many useful discussions which have improved this work. The simulations reported here were run on the Llaima Cluster at the University of Victoria, and on the McKenzie Cluster at the Canadian Institute for Theoretical Astrophysics. This work has been supported by various grants to JFN and a post-graduate scholarship to ADL from Canada’s NSERC. AH gratefully acknowledges financial support from NOVA and NWO.

REFERENCES

- Balogh, M.L., Navarro, J.F., Morris, S.L., 2000, *ApJ*, 540, 113
 Bertschinger, E., 1985, *ApJS*, 58, 39
 Benson, A. J., 2005, *MNRAS*, 358, 551
 Colless, M., et al. 2001, *MNRAS*, 328, 1039C
 Davis, M., Efstathiou, G., Frenk, C.S., White, S.D.M., 1985, *ApJ*, 292, 371
 De Lucia, G., Kauffmann, G., Springel, V., White, S.D.M., Lanzoni, B., Stoehr, F., Tormen, G., Yoshida, N., 2004, *MNRAS*, 348, 333D
 Diemand, J., Moore, B., Stadel, J., 2004, *MNRAS*, 352, 535D
 Diemand, J., Kuhlen, M. Madau, P., 2007, *ApJ*, 657, 262D
 Diemand, J., Kuhlen, M. Madau, P., 2007, *ApJ*, 667, 859D
 Eke, V.R., Cole, S., Frenk, C.S., 1996, *MNRAS*, 282, 263
 Einasto, J., Trudy Inst. Astrofiz. Alma-Ata, 1965, 51, 87
 Gao, L., White, S.D.M., Jenkins, A., Stoehr, F., Springel, S., 2004, *MNRAS*, 355, 819G
 Gao, L., Springel, S., White, S.D.M., 2005, *MNRAS*, 363L, 66G
 Gao, L., Navarro, J.F., Cole, S., Frenk, C.S., White, S.D.M., Springel V., Jenkins A., Neto A., 2007, arXiv:07110746
 Ghigna, S., Moore, B., Governato, F., Lake, G. Quinn, T., Stadel, J., 1999, *asp* 176, 140G
 Ghigna, S., Moore, B., Governato, F., Lake, G. Quinn, T., Stadel, J., 1998, *MNRAS* 300, 146
 Gill, S.P.D., Knebe, A., Gibson, B.K., *MNRAS*, 356, 1327
 Helmi, A., White, S.D.M., Springel, V., 2002, *PhRvD*, 66f, 3502H
 Jing, Y.P., Suto, Y., Mo, H.J., 2007, *ApJ*, 657, 664J
 Kallivayalil, N, van der Marel, R.P., Alcock, C., *ApJ*, 2006, 652, 1213K
 Klypin, A., Kravstov, A.V., Valenzuela, O., Prada, F., 1999, *ApJ*, 522, 82
 Kravstov, A.V., Gnedin, O.Y., Klypin, A.A., *ApJ*, 609, 482K
 Kroupa, P., Thies, C., Boily, C.M., 2005, *Å*, 431, 517
 Kunkel, W.E., Demers, S., 1976, *R. Greenwhich Obser. Bull.*, 182, 241
 Libeskind, N.I., Cole, S., Frenk, C.S., Okamoto, T., Jenkins, A., 2007, *MNRAS*, 374, 16
 Li & Helmi, 2007, on the arXiv, accepted to *MNRAS*, On the Infall of Subhalos in Groups
 Lynden-Bell, D., 1976, *MNRAS*, 174, 695
 Lynden-Bell, D., 1982, *Obs*, 102, 202
 Mamon, G.A., Sanchis, T., Salvador-Solé, E., Solanes, J.M., *Å*, 414, 445
 Merritt, D., Navarro, J.F., Ludlow, A., Jenkins, A., 2005, *ApJ*, 624, 85
 Merritt, D., Graham, A.W., Moore, B., Diemand, J., Terzić B., 2006, *AJ*, 132, 2685
 Moore, B., Ghigna, S., Governato, F., Lake, G., Quinn, T., Stadel, J., Tozzi, P., 1999, *ApJ*, 524, L19
 Navarro, J., Hayashi, E., Power, C., Jenkins, A.R., Frenk, C.S., White, S.D.M., Springel, V., Stadel, J., Quinn, T.R. 2004, *MNRAS*, 349, 1039N
 Navarro, J.F., White, S.D.M., 1993, *MNRAS*, 265, 271
 Piatek, S., Pryor, C., Olszewski, E. W., 2007, arXiv:07121764
 Power, C., Navarro, J.F., Jenkins, A.R., Frenk, C.S., White, S.D.M., Springel, V., Stadel, J., Quinn, T., *MNRAS*, 338, 14P
 Sales, L.V., Navarro, J.F., Abadi, M.G., Stienmetz, M., 2007, *MNRAS*, 379, 1464
 Sales, L.V., Navarro, J.F., Abadi, M.G., Stienmetz, M., 2007, *MNRAS*, 379, 1475S
 Springel, V., White, S.D.M., Tormen, G., Kauffmann, G., 2001, *MNRAS*, 328, 726S
 Springel, V. 2005, *MNRAS*, 364, 1105S

TABLE 1
PROPERTIES OF SIMULATED HALOS USED IN THIS STUDY.

Halo	ϵ_G [h^{-1} kpc]	M_{200} [$h^{-1}M_\odot$]	$M_{\text{DM}}^{\text{assoc}}$ [$h^{-1}M_\odot$]	r_{200} [h^{-1} kpc]	V_{max} [km s^{-1}]	r_{max} [h^{-1} kpc]	N_{200}	$M_{\text{sub}}^{\text{assoc}}$ [$h^{-1}M_\odot$]	N_{sub} [assoc]	N_{sub} ($r < r_{200}$)	N_{sub} ($r < r_{100}$)	N_{sub} ($r < r_{50}$)	N_{sub} $r_{\text{apo}} > 2.5r_{\text{ta}}$
9-1-53	0.250	9.17×10^{11}	12.0×10^{11}	158.0	184.8	36.0	3.24e6	0.89×10^{11}	904	513	742	1017	3
9-12-46	0.181	6.44×10^{11}	9.79×10^{11}	140.4	159.9	34.9	4.82e6	0.47×10^{11}	2020	865	1314	1828	14
9-13-74	0.220	8.76×10^{11}	12.4×10^{11}	155.6	175.9	32.0	4.18e6	1.04×10^{11}	1683	831	1232	1645	15
9-14-39	0.186	12.6×10^{11}	17.9×10^{11}	175.7	203.5	37.8	3.30e6	1.27×10^{11}	1416	594	1050	1581	4
9-14-56	0.275	8.57×10^{11}	12.2×10^{11}	154.4	178.6	33.7	2.61e6	1.00×10^{11}	1160	469	646	930	12

TABLE 2
DYNAMICAL PROPERTIES OF SUBHALO POPULATION

Sample	N_{sub} [5 sims]	n_0 [arb.units]	r_{-2} [r_{200}]	r_{h} [r_{200}]	α	$\langle \beta \rangle$	$\langle \sigma_r \rangle$ [V_{200}]
Assoc. dark matter		5422	0.112	0.558	0.159	0.270	0.734
Assoc. subhalos	7183	4691.0	1.08	1.09	0.842	0.053	0.712
($X = V_{\text{max}}^{\text{acc}}/V_{200}$)							
$X > 0.170$	150	42848.5	0.70	0.70	0.352	0.059	0.699
$0.063 < X < 0.17$	2110	3709.2	0.80	0.87	0.754	0.091	0.712
$0.040 < X < 0.063$	2110	875.9	1.09	1.10	0.991	0.018	0.699
$0.025 < X < 0.040$	750	222.0	1.26	1.39	1.001	0.034	0.762
($Y = \log_{10} M_{\text{sub}}/M_{200}$)							
$Y > -3.3$	150	28.3	1.12	1.14	1.536	0.207	0.769
$-4.6 < Y < -3.3$	1918	1181.3	0.99	1.06	0.886	-0.001	0.723
$-5.1 < Y < -4.6$	1918	1275.5	1.11	1.08	0.897	0.021	0.735
$-5.42 < Y < -5.1$	750	341.6	1.09	1.13	0.939	-0.028	0.708

Spergel, D.N., et al. 2003, ApJ, 148, 175S
Taylor, J. E., Babul, A., 2005, MNRAS, 364, 515T
Taylor, J. E., Babul, A., 2005, MNRAS, 464, 535T
Toomre, A., Toomre, J., 1972, ApJ, 178, 623
van Albada, T.S., 1982, MNRAS, 201, 939V
Wang, H.Y., Mo, H.J., Jing, Y.P., 2007, MNRAS, 375, 633

White, S.D.M., Navarro, J.F., Evrard, A.E., Frenk, C.S., 1993,
nature, 366 429
Zhu, G., Zheng, Z., Lin, W.P., Jing, Y.P., Kang, X., Gao, L., 2006,
ApJ, 639L 5Z